Optical transmission of ferrofluids exposed to a magnetic field: analysis by electromagnetic wave propagation numerical methods

Ángel SANZ-FELIPE [(1)], Ismael BARBA [(2)], Juan Carlos MARTÍN [(1,*)]

1. Applied Physics Dept., University of Zaragoza, C/ Pedro Cerbuna, 12, 50009 Zaragoza (Spain).
2. Electricity and Electronics Dept., University of Valladolid, Paseo de Belén s/n, 47071 Valladolid (Spain).

*Corresponding author

Abstract

Optical transmission changes in ferrofluids when exposed to magnetic fields are difficult to predict: under similar conditions, exposure to a magnetic field may cause increasing, decreasing or even non monotonous optical transmission evolution in different samples. Absence or presence of coalescence has been conjectured as the key phenomenon that causes the different behaviors, but to our knowledge without any theoretical support. In the first part of this work, experimental data are provided in order to illustrate the different possible trends that may be observed. In the second part, a set of some thousands of particles is considered in different arrangements: distributed at random, grouped in single chains or with aggregates of several chains. The optical transmission of each arrangement is obtained by means of the CST software. The numerical results obtained provide a theoretical connection between the optical transmission experimental trends observed and the processes of chain formation and aggregation by coalescence, which facilitates a much deeper understanding of the phenomena observed.

1. Introduction

Ferrofluids are colloidal suspensions whose continuous phase is liquid and whose dispersed phase is magnetic nanoparticles. In presence of magnetic field, they tend to gather in chains parallel to the field lines or in more complex aggregates due to coalescence of these chains [1]. These phenomena induce changes in these media optical properties: their optical absorption varies and dichroism and even rotatory power appear in some particular cases [2–4]. Control of these properties by the applied magnetic field makes ferrofluids interesting as basic functional media of different photonic applications: variable attenuators, polarizers or isolators, optical magnetic field sensors, etc [5–9]. These behaviors recall other magneto-optical phenomena such as the Faraday and the Kerr effects, although they have a different nature, based on the Zeeman effect [10], while the magneto-optical behavior of ferrofluids is explained by simple nanoparticle rearrangement.

Predicting the magneto-optical behavior of a ferrofluid constitutes a very demanding challenge. Once the magnetic field is applied, the colloid optical response (magnitude and speed) depends on many factors, some of them measurable by well-known techniques, some others very difficult to obtain. Amongst the first, we can cite

nanoparticle concentration, size and magnetization, as well as fluid viscosity. Amongst the second: for mixture stability, it is usual to add a polymer during the nanoparticles synthesis process, which adheres to the magnetic core in a rather unpredictable way. This coating has a strong influence both on the chain formation, as it limits neighbor nanoparticles closeness, and on the optical scattering caused by isolated particles or chains of them. The same way, usually a surfactant is added to the mixture, in order to avoid particles aggregation and subsequent precipitation: the surfactant adheres to the polymer causing electrostatic repulsion between particles. Modelling this electrostatic contribution would be desirable for nanoparticle interaction analysis, but this treatment must deal with lack of knowledge about both charge density magnitude and distribution around a nanoparticle (of course, the different shapes and sizes of each nanoparticle, coated with polymer and surrounded by surfactant, should be somewhat averaged in order to get a manageable model).

This complexity justifies the variety of magneto-optical responses reported in the literature, even with opposite trends under similar stimuli. Consider a ferrofluid and a light beam which propagates through it: if a magnetic field is applied in the light beam direction, the ferrofluid optical transmission may reduce [11–13] or increase [11,12,14]. Even with the same sample, both diminution and growth can be observed depending on the magnetostatic field intensity [1]. Besides, this trend dependence on the magnetostatic field is also obtained for light beam perpendicular to it [2]. It has also been reported that similar experiments with different light wavelengths provide opposite trends [15]. The aim of this work is to provide structure to these different behaviors: on the one hand, to identify the key factors that determine the optical transmission evolution trend in a given sample and on the other hand to justify them on a theoretical basis, not simply on correlations between samples features and their responses.

Some authors have suggested that these trends depend on the coalescence amount [1,16–19], with several considerations to be pointed out. On the one hand, there are different ways to refer to the same phenomenon. In [18], the term columnar phase transition is preferred to coalescence. In [19], the effect is explained by referring to a competition between dipole-dipole and Van der Waals forces. Obviously, if the latter are intense enough, coalescence takes place, but this term does not appear in [19]. On the other hand, whether coalescence increases or decreases transmission has not been clearly stated, to our knowledge. And, most of all, the different suggestions have not been given any theoretical support, save for [18], which will be commented later. For all these reasons, we think that coalescence as the key phenomenon for understanding these behaviors is still a hypothesis. This study is aimed at proving it. Besides, there are other works which show how the amount of the optical transmission changes depends on factors such as particle size or wavelength [20]. Of course these factors do have a quantitative influence, but our hypothesis is that the influence of coalescence is qualitative, mainly for light beam parallel to the magnetostatic field: coalescence appearance reverses the trend.

Several models have been proposed for the magneto-optical response of ferrofluids. These works provide a basis for our study, although they are aimed at other purposes and do not establish clearly the reason why different trends exist. Some models provide a description of the phenomena observed by resourcing to any fitting parameter. An example of this group of approaches is [21], which considers an effective concentration of the liquid phase as a function of the magnetic field. As fitting

parameters are only determined after the experiments, these models do not have predictive capability and, therefore, they cannot be used in order to anticipate the magneto-optical behavior of a given sample. Just a few works provide models without fitting parameters and, therefore, with predictive capacities. In [22], nanoparticle arrangements are calculated by the Monte-Carlo method and Mie's theory is applied to calculate the sample transmission, but this study does not analyze cases with different trends. In [18], phase condensation models are considered to predict chain organization and the sample transmission is also calculated by Mie's theory, applied to a chain of spheres or to cylinders. For light beam perpendicular to the applied magnetostatic field, Mie's resonances explain the trend reversals in the experimental series presented. For light beam parallel to the field, no analysis is presented.

The model employed here follows a scheme similar to the above mentioned ones. In its first stage, it calculates particle evolution from a random distribution to an arrangement in chains, by means of a method previously developed by us [23]. In its second stage, optical transmission of the samples is calculated by an electromagnetic wave propagation numerical method. To our knowledge, no methods of this kind had been applied for ferrofluid optical transmission calculations yet. This way, no simplified model is employed at this stage, and the whole complexity of each particular distribution is taken into account. Besides, the calculations selected are focused on the hypothesis to be tested: distributions with isolated chains and with the same chains grouped by two or by three have been considered, in order to isolate the coalescence effect on the optical transmission. This approach has proved to be helpful in order to clear up the causes of the different trends observed.

In Section 2, we provide experimental results illustrating the different possible trends. Section 3 is devoted to optical transmission numerical calculations of a set of nanoparticles arranged in different ways: completely scattered, in isolated chains or with some of these chains coalesced. Comparison of the different results allows us to precise the trends of optical transmission evolution, both in absence and presence of coalescence. This knowledge allows us to explain Section 2 results.

2. Experiments

The experimental setup employed can be found in [24] and is standard for magneto-optical measurements. Two Helmholtz coils (radius, 16.5cm) connected to a DC power supply provide the magnetic field. In the center of this configuration, an optical glass cuvette containing a ferrofluid sample is placed. The cuvette inner dimensions are 9.5mm × 36.8mm × 2mm (from now on called a, b, and c, respectively). The cuvette is illuminated by a He-Ne laser beam (λ = 632.8nm). Its orientation is perpendicular to the faces with dimensions $a \times b$, so that it propagates along a ferrofluid thickness c. This beam is expanded in order to illuminate a sample section as wide as possible (beam diameter a), so that local sample inhomogeneities effects are minimized. Light that has traversed the sample is focused into a PIN photodetector. The Helmholtz coils can be rotated so that the magnetic field at the sample position may point out either in parallel or perpendicular direction with regard to the laser beam orientation.

In the results shown next, the samples have been shaken in order to minimize the presence of aggregates, either originated by spontaneous clustering or by sample exposure to magnetic field in previous measurements. At $t = 0$, the power supply is switched on and a DC current is established. The magnetic field intensity in the cuvette position is 72G.

Three samples have been employed. Available information is listed in Table I. TEM images of sample#1 nanoparticles can be found in [24]. The magnetic core presents a certain cubic shape without a preferred direction, surrounded by the irregular coating. A low statistical size dispersion is frequently guaranteed by the manufacturers in order to be as monodisperse as possible face to their potential applications. For instance, sample#1 has a PdI of 0.176, a value whereby the size distribution can be considered almost monodisperse. Therefore, since our aim is qualitatively analyzing whether transmission increases or decreases when the sample is exposed to a magnetic field, the nanoparticles will be considered statistically as identical spheres in their subsequent analysis presented in Section 3. For a more precise quantitative study, both nanoparticles shape and size dispersion should be taken into account.

Table I. – Available information on the samples employed. D_h: particle hydrodynamic diameter.

	Sample#1	**Sample#2**	**Sample#3**
Magnetic core composition	Fe_3O_4	Fe_3O_4	$Co_{0.77}Fe_{2.23}O_4$
Agents added	SDS	No information. Possibly coating worn out due to aging	Oleic acid
D_h(nm)	184	35	12
Liquid phase	Water	Water	Hexane

Together with these data, it is significant for our purposes to observe the sample with a camera. The setup for this aim is the above described, substituting the photodetector by a CMOS camera, and using the lens (the one which focused the laser beam into the photodetector) to form the sample image on the camera sensor. Figure 1 shows an image of both samples#1, #2 and #3 in presence of magnetic field. In sample#1, Figure 1a, no aggregates can be seen either before or after magnetic field application (therefore, if present their dimensions are smaller than the optical setup resolution: 2.75 μm/px). A speckle pattern is observed due to the mutual interference of the wavefronts scattered by each particle or small aggregates of them. In contrast, aggregates in sample#2 after few seconds of magnetic field application are visible, and once the magnetic field is switched off, it is necessary to shake it repeatedly in order that aggregates are not visible. Horizontal chains 20-50 μm thick and up to 1 mm long are observed (dark areas). Concerning the aggregation properties of sample#3, a clear aging process has been detected in this sample: first, no aggregates have been seen as in sample#1 occurs, but few days later and after several series of measurements, small chains 0.1-0.2 mm long began to be observed, as shown in Figure 1c. This image

corresponds to just $t = 0.08$ s after the magnetic field is turned on, showing how fast the process is in this case. This aging process on the particles coating will be studied in subsection 2.1.

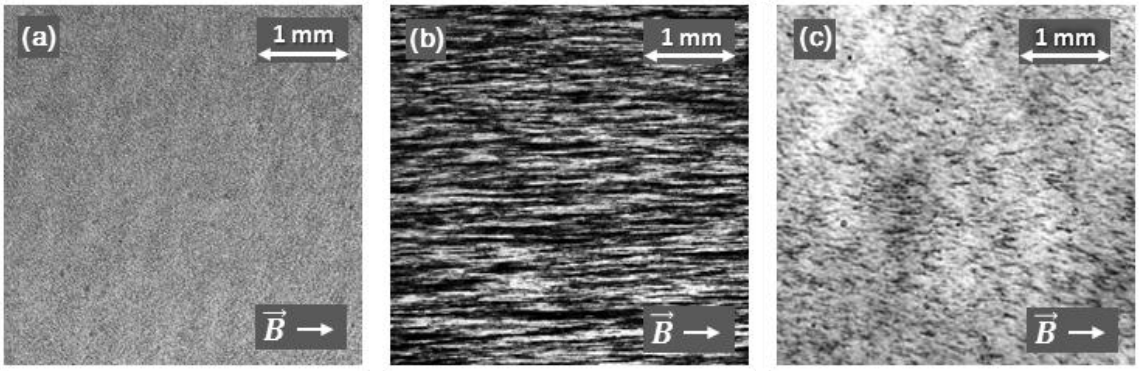

Figure 1.– Sample#1 (a), sample#2 (b) and sample#3 (c) images, with applied magnetic field. The image corresponding to sample#3 presents the small chains observed after aging effects.

2.1. Magnetic field parallel to the laser beam

Figure 2 shows the optical transmission evolution of different ferrofluid samples. Various evolution rates and trends can be appreciated. Remark that the smaller the particles and the less viscous the liquid phase, the faster the evolution rate. As hexane is less viscous than water, sample#3 evolution speed is doubly favored with regard to the other samples, both by particle size and by viscosity.

Explaining the cause of the diversity in the trends found constitutes the aim of this work and it will be developed along Section 3. In this one, simply remark that the overall trends in samples#1 and #2 are opposite. Also interesting, some of these curves are not monotonous, with a change in trend that can be smooth over time (Figure 2a) or sharp (Figure 2b, inset). Other authors have already reported similar reversals [2,12,16]. As shown in Figure 2(a), the higher the concentration, the earlier the trend reversal appearance. This concentration influence will be discussed in Section 3.

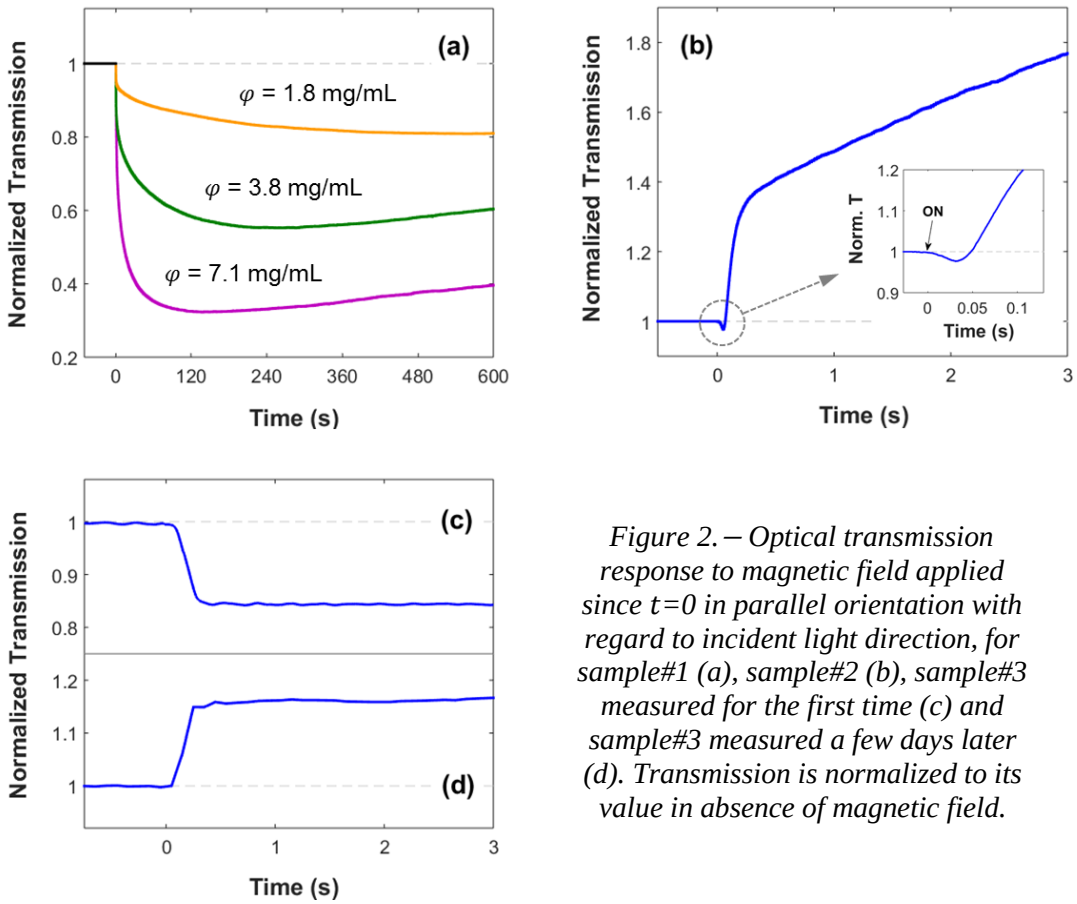

Figure 2.– Optical transmission response to magnetic field applied since t=0 in parallel orientation with regard to incident light direction, for sample#1 (a), sample#2 (b), sample#3 measured for the first time (c) and sample#3 measured a few days later (d). Transmission is normalized to its value in absence of magnetic field.

Samples#1 and #2 responses were repetitive in series of measurements carried out within a time lapse of days. Nevertheless, sample#3 showed a gradual change in its response. Figure 2c corresponds to the first measurement carried out with sample#3, while Figure 2d shows its response a few days later, after several series of measurements. Remarkably, in the state corresponding to Figure 2c, no aggregate was noticeable while, in the one corresponding to Figure 2d, aggregates were visible. We attribute this evolution to the aging process on the polymeric coating mentioned above. At the first measurements, particles had a polymeric shell that attenuated aggregation. However, when the coating suffered some wear, it could have lost its stabilizing properties. Thus, in subsequent exposures to magnetic field they aligned with a shorter distance between particles, which eased aggregation and coalescence. As a consequence, the magnitude and trend of the transmission changes were altered despite using the same measurement conditions. A trend inversion is observed between Figures 2c and 2d related to this effect [18,25]. Results point out towards a decreasing optical transmission evolution in absence of coalescence (sample#1 and sample#3, Figure 2c) and increasing in presence of it (sample#2 and sample#3, Figure 2d). Anyway, this idea will be cleared up in Section 3.

2.2. Magnetic field perpendicular to the laser beam

Figure 3 shows transmission evolutions for magnetic field perpendicular to the laser beam. For sample#1, there is a noticeable difference depending on the beam polarization orientation: electric field parallel or perpendicular to the applied magnetic field (so, to the particle chains). Nevertheless, for sample#2 no polarization dependence

is observed. According to scattering theory, noticeability of polarization dependence has to do with the scatterer's size. Theory on light scattering by a cylinder perpendicular to light propagation points out that polarization dependence tends to disappear if the cylinder radius is much greater than the light wavelength [26]. According to the aggregate sizes observed in sample#2 (roughly cylinders with 20-50 μm diameters, Figure 1b), absence of polarization dependence is logical. By contrast, sample#1 chains are not visible (Figure 1a), so they must be smaller than the camera resolution (2.75 μm/px), leading to a dependence on polarization.

Concerning sample#3, no results are shown because transmission changes were unnoticeable.

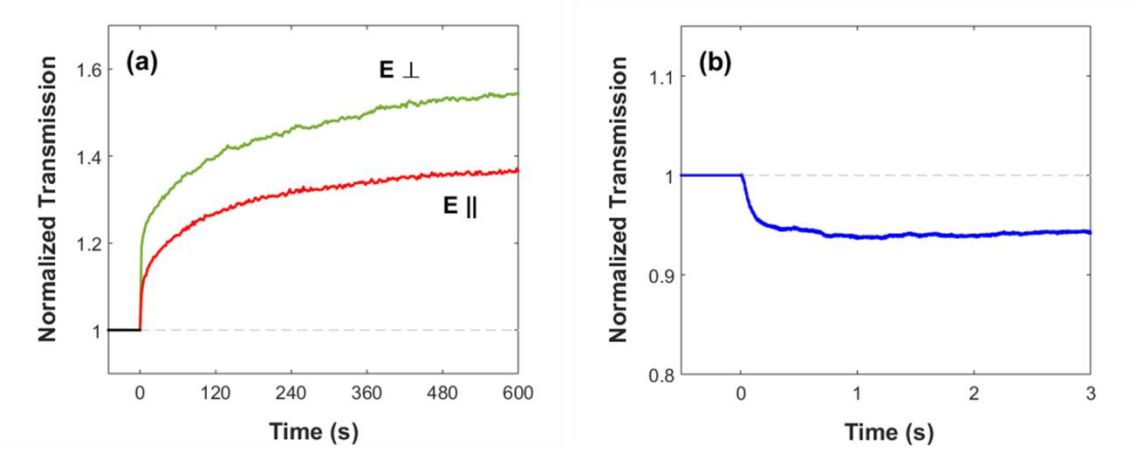

Figure 3.– Optical transmission response of sample#1 (φ=7,1mg/mL) (a) and sample#2 (b), to magnetic field applied in perpendicular orientation with regard to incident light direction.

3. Numerical analysis

As finding a qualitative, intuitive explanation to all these behaviors is not evident, we resource to numerical calculations in order to analyze them. The idea is to compare the optical transmissions of the same set of nanoparticles (within a fluid) arranged in different ways, corresponding to absence or presence of magnetic field, and in this latter case, with or without coalescence. Particles in our simulations are identical spheres in order to simplify their modeling. An inner sphere representing the magnetic material, surrounded by a shell representing the polymer coating, constitutes the particles considered. We assign to the inner sphere the complex permittivity 5.5489-0.6947j, corresponding to magnetite at $\lambda = 632.8$nm [27] (wavelength employed in Section 2 measurements). For the shell, the permittivity considered is 2.13, within the typical polymer permittivity values within the visible range. Finally, permittivity chosen for the mixture continuous phase is 1.7734, corresponding to water at $\lambda = 632.8$nm [28]. A quantitatively precise value of the attenuation is not expected since the simulated particles do not strictly reflect the shape of the experimental ones. Furthermore, consider the sample#1: the coating is formed by a complex structure of polymer, SDS micelles and even solvated water [24], so that an effective permittivity could not be assured even knowing each component permittivity. The only solution would be to retouch every parameter by repeating simulations, which would require a long

calculation time. For that reason, our results will focus on analyzing the qualitative trends when the chains are formed or coalesced.

Table II. – Summary of the different particle distributions considered.

Reference samples	Isolated chains	Coalescence
A1: R=92nm	**A2**: d=146nm	**A3**
	A2': d=50nm	
B1: R=83,5nm	**B2**: d=146nm	**B3**

The different particle distributions considered have been configured as summarized in Table II and explained next:

1) Reference samples A1 and B1 have been generated by sewing particles at random within each cell. The particle distribution is the same in both samples, Figure 4a. Particle size is an important parameter studied in the literature [29,30]. It determines the magnetic response and mobility of the particles, and therefore the optical response. However, the distinction on the contribution of the coating to the optical effects is not frequently analyzed separately [2]. For this reason we generate these two reference samples: the only difference between them is the particle outer shell radius R. The inner magnetic core diameter is 50 nm. These samples represent the ferrofluid in absence of magnetic field, and so the initial situation of the ferrofluid ($t = 0$).

2) A computer program developed by us, which simulates evolution of the nanoparticle distribution present in a ferrofluid after magnetic field switch-on [23], is employed to calculate how particles group into chains, departing from the reference sample distributions. The program allows one to choose the equilibrium distance between the outer surfaces of consecutive particles in a chain, d. A magnetic field intensity of 72 G has been applied to the reference distribution as the initial step of the particles evolution ($t = 0$), and maintained during the whole simulation. Numerical calculation has been carried out with the program parameters indicated in [23]. Stability in chain formation was sufficiently reached, Figure 4b. This stability does not take into account chains coalescence as will be clarify in the next point. Evolution departing from sample A1 has been calculated for two equilibrium distances, which has led to A2 and A2' distributions. B2 has been generated departing from B1.

3) The model to calculate the interaction between nanoparticles does not account for coalescence [23], so that it just simulates its evolution at early stages after application magnetic field application. Departing from the configurations generated in 2), some chains are moved to form groups of chains, as it happens as a result of coalescence. In this case the evolution from stage 2) to stage 3) is not the result of any calculation: simply the coordinates of some chains observed in stage 2) are modified by us in order to simulate that several chains come together. Specifically, the groups of chains have two or three of them, so that the coalescence represented is relatively small (for instance, sample#2 aggregates in

Figure 1 must contain at least some hundreds of chains). In this way, A3 and B3 have been generated departing from A2 and B2, respectively.

Samples in Table II have been considered to be related to the experimental samples as follows. Sample A1 has been generated departing from sample#1 characteristics, so that A2 and A3 would refer respectively to the initial response and the next evolution when coalescence begins to be significant in order to verify whether it is related to the observed trend inversion (Figure 2a). Samples A2' and B1 to B3 have been carried out to test the differences that one can expect when particles are chained with a shorter distance between them or with a smaller volume of coating respectively. The latter situations would refer to the wear of the coating and its insufficient stabilizing action, as it may occurs in samples#2 and #3.

The volume considered for the simulation is a parallelepiped, result of concatenating 22 cubic cells with 5.2μm edge (Figure 4). The total number of particles inside is 4004 (182 at each cell, equivalent to 7.1mg/mL concentration). In order to simulate a more realistic sample and to avoid any repeating pattern, every concatenated cubic cell undergoes a random displacement in a random direction transverse to the concatenation one. Light propagates along the concatenation orientation, Figure 4c.

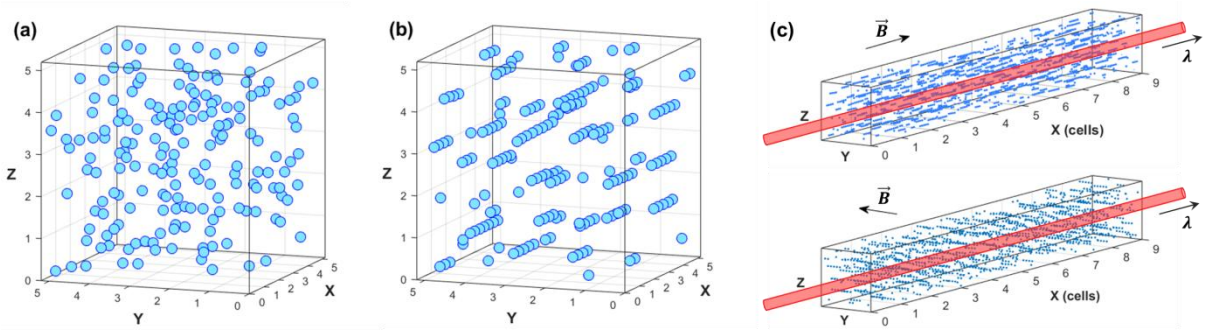

Figure 4.– Simulated ferrofluid cubic cell with (a) a set of randomly distributed particles and (b) the isolated chains obtained with the program. These figures correspond to samples A1 an A2 respectively. (c) Concatenation of cells along the light propagation direction with magnetic field parallel (up) and perpendicular (down) with regard to light direction.

Optical transmission calculation of each particle distribution is carried out by means of the CST Studio Suite® software. This software allows one to define a mesh of points filling a certain volume and to assign a complex permittivity to each point, depending on the specific material that corresponds to it: magnetite, polymer or water. The program distributes nodes, minimizing their density in continuous regions and guaranteeing a distance between consecutive nodes of 16 to 30 nm. In order to prevent numerical reflections in the domain limits, absorbing walls are defined in the volume faces perpendicular to the light orientation, and magnetic or electric walls in the volume faces parallel to it (according to the input light polarization). Time-domain propagation of an input Gaussian pulse along the cells is calculated, Figure 5. The pulse spectrum is centered at 632.8nm and introduced to the simulation volume at the input wall ($x = 0$). Then, transmitted and reflected waves are detected at the output wall ($x = 114.4$ μm, corresponding to the total length of 22 concatenated cells) and at the input wall

respectively. Figure 5b shows the three waves registered. The frequency-dependent transmission calculation involves the Fourier transforms of the transmitted and incident pulses. Optical transmission of the sample is then calculated as the quotient between the transmitted and incident waves as a function of the wavelength. Besides, a similar frequency-dependent reflection calculation is carried out simply as a check of simulation correctness. Figure 6 shows the transmission and reflection spectra obtained for sample A1. The power attenuation of the sample can be calculated by squaring this result (it has been shown as electric field amplitude in order to better see the reflected signal behavior). The intensity reflected by the particles is negligible, so that all the incident light is transmitted or extinguished (either by scattering and/or by absorption).

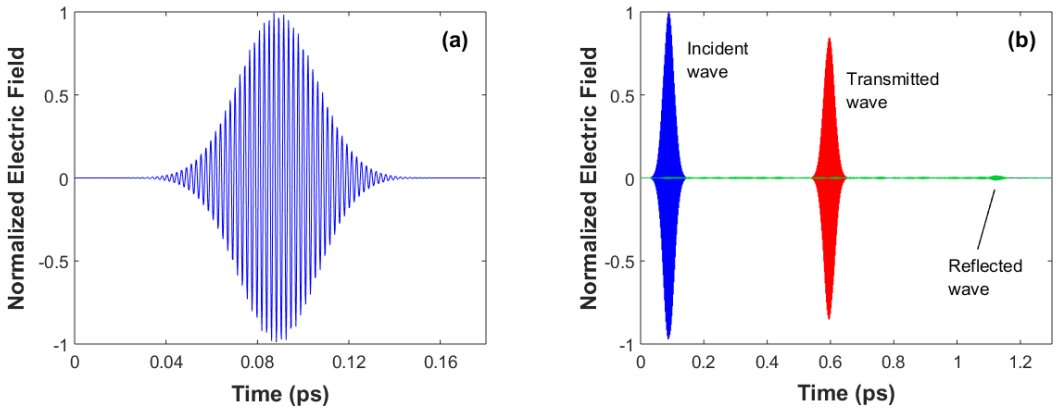

Figure 5.– (a) Incident Gaussian pulse and (b) transmitted and reflected waves calculated for sample A1.

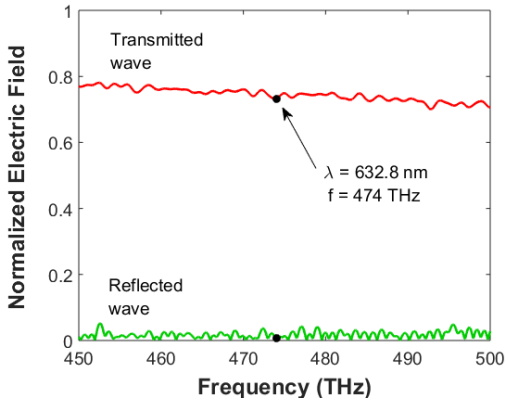

Figure 6.– Frequency-dependent electric field amplitude of the transmitted and reflected waves calculated for sample A1, normalized to the incident amplitude.

Both the nanoparticles characteristic values and the calculation domain volume have been chosen in order to get a compromise between different requirements: the longer the propagation length and the greater the nanoparticle size and concentration, the greater the optical power loss and so, the greater the calculation precision. Nevertheless, take into account that with the calculation domain chosen, each propagation calculation requires computing times of several tens of hours; if the propagation length was raised, the computing time would also increase, much sharply than in a simple linear way. On the other hand, particle size and concentration must be within a reasonable range of values. Considering all these ideas, particle size selected

for these simulations is that of sample#1, with the maximum concentration shown in Figure 2a.

3.1. Magnetic field parallel to light beam

Table III presents the normalized transmission results obtained for magnetic field parallel to the light beam. T(XN) is the sample transmission at stage N divided by the respective sample transmission at stage 1 (X=A or B; N=2, 2' or 3).

Table III. – Sample normalized transmissions for magnetic field parallel to light orientation.

Isolated chains		**Coalescence**	
T(A2)	0.91	T(A3)	1.08
T(A2')	0.78		
T(B2)	0.90	T(B3)	1.02

These results show several interesting features. Configuration in isolated chains gives rise to a decrease in optical transmission, with regard to the random configuration corresponding to absence of magnetic field. In contrast, chain coalescence is enough to reverse the trend and make optical transmission increase. Obviously, coalescence must always be preceded by isolated chains formation. Therefore, according to this scheme, there must be a first stage where optical transmission decreases and, at some moment, the trend may be reversed if there is enough coalescence, and a second stage where optical transmission increases can be observed. This scheme consisting of associating optical transmission decrease with predominance of isolated chains and increase with symptom of coalescence matches perfectly with the experimental results found:

- In Figure 2a (sample#1), the lower concentration curves shows just the decreasing stage, while the second stage appears faster and faster with increasing concentration. This is coherent: the higher the concentration, the stronger the coalescence. Figure 7 shows a more detailed series of measurements. In Figure 7a, it can be appreciated how the higher the concentration, the sooner the curve reaches its minimum. This can also be observed in Figure 7b, together with another trend reversal due to coalescence: in Figure 7a, the higher the concentration, the lower the optical transmission (isolated chains dominate), while in Figure 7b the opposite is observed (coalescence dominates).

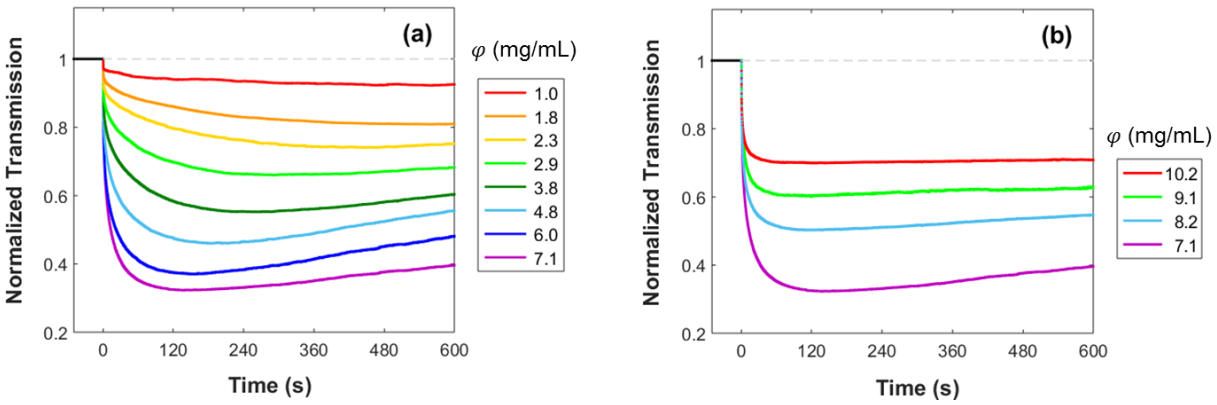

Figure 7.– Sample#1 optical transmission response for different particle concentration below (a) and above (b) a critical concentration of 7.1 mg/mL in which a trend reversal in parallel magnetic field orientation is observed.

- In Figure 2b (sample#2), there is also a first decreasing stage, but it might remain unnoticed depending on the time scale employed. The second stage almost fills the whole time range considered. In this sample, coalescence is much stronger than in sample#1 (Figure 1), which causes a rapid optical transmission growth. Besides, the rate of optical transmission evolution is greater than for sample#1 because particles in sample#2 are smaller than in sample#1.

- The different behavior of sample#3, illustrated in Figure 2c and 2d, may be attributed to the mentioned aging process, and so to a gradual loss or wear of the particles' polymer coating due to repetitive measurements. When polymer is around particles, coalescence is more difficult and sample#3 behaves like sample#1: its optical transmission decreases, as it corresponds to formation of isolated chains. Nevertheless, once the polymeric shell disappears, sample#3 behaves like sample#2: stage 1 is not noticeable and just the optical transmission growing corresponding to stage 2 appears. Again, the fast evolution rate observed in this sample, compared with the other two, is explained by the particle sizes and carrier fluid's viscosity of each sample.

It is also worthwhile to remark the influence of the distance d: this is the only parameter that differences cases A2 and A2' and the variations in their optical transmissions are notable. Take into account that d is difficult to foresee even though the mixture composition is well defined because it depends on the surfactant action, not quantifiable by means of any model. This is one of the multiple reasons why, even though the mixture composition is well determined, a precise, quantitative prediction of its magneto-optical response is a very demanding task. On the other hand, comparison between A2 and B2 results points out that the outer shell size does not have a significant influence on the magnitude of the transmission changes studied here.

3.2. Magnetic field perpendicular to light beam

Table IV presents the results obtained for magnetic field in perpendicular orientation with regard to light propagation. Transmission is calculated in two cases,

corresponding to the input wave electric field with parallel or perpendicular polarization with regard to the magnetic field (and particle alignment) orientation.

Table IV. – Sample normalized transmissions for magnetic field perpendicular to light orientation and for two polarizations of the incident electric field: parallel (∥) and perpendicular (⊥) to the applied magnetic field.

Isolated chains			**Coalescence**		
	$E \parallel$	$E \perp$		$E \parallel$	$E \perp$
T(A2)	1.18	1.22	T(A3)	1.20	1.31
T(A2')	0.96	1.11			
T(B2)	0.99	1.06	T(B3)	1.12	1.21

Results obtained show in all cases that optical transmission is greater for perpendicular than for parallel polarization, in agreement with Figure 3a. Also in all cases calculated, coalescence makes transmission grow. Concerning isolated chains formation, a growing trend is obtained for perpendicular polarization in all cases, while for parallel polarization the relative transmission may be greater or lower than unity. The greater the R and d values (A2 sample), the higher the transmission. When comparing samples#1 and #2, take into account that coalescence would favor a greater relative transmission for sample#2 but R and d values would favor the opposite (in sample#2, the strong coalescence observed points out towards a very small polymeric shell, which means low R and d values). So, even with a complete sample characterization, the change in transmission for this magnetic field orientation is really difficult to anticipate.

Conclusions

Concerning ferrofluid optical transmission for magnetic field parallel to the light beam orientation, numerical results show that formation of isolated chains give rise to transmission decrease, while coalescence causes transmission increase. With this basic idea, the different experimental evolutions of ferrofluid optical transmissions after magnetic field application can be explained: at a first stage just simple chains begin to form and optical transmission decreases; if coalescence is strong enough, a second stage takes place in which optical transmission increases. In some experiments carried out with samples presenting strong coalescence, the first step may not be appreciated due to the time scale employed for evolution tracking, so just a monotonous increase is observed. Specifically, as coalescence intensity is conditioned by particle concentration, this parameter has a strong influence on the magnitude and duration of each stage.

Concerning magnetic field perpendicular to the light beam orientation, numerical results support the appearance of dichroism, with greater transmission for perpendicular than for parallel polarization, with regard to the applied magnetostatic field. The different cases calculated also justify the various possible trends in the optical transmission evolution, as it is shown that they are conditioned by the particle

polymeric shell size. Anyway, if coalescence appears, it favors optical transmission increase.

Acknowledgements

This work has been supported by the Diputación General de Aragón, project E44_17R.

REFERENCES

[1] Ivey M., Liu J., Zhu Y., and Cutillas S., "*Magnetic-field-induced structural transitions in a ferrofluid emulsion*", Phys. Rev. E **63** (2000) 011403.

[2] Brojabasi S., Muthukumaran T., Laskar J.M., and Philip J., "*The effect of suspended Fe_3O_4 nanoparticle size on magneto-optical properties of ferrofluids*", Opt. Commun. **336** (2015) 278–285.

[3] Vales-Pinzón C., Alvarado-Gil J.J., Medina-Esquivel R., and Martínez-Torres P., "*Polarized light transmission in ferrofluids loaded with carbon nanotubes in the presence of a uniform magnetic field*", J. Magn. Magn. Mater. **369** (2014) 114–121.

[4] Raşa M., "*Improved formulas for magneto-optical effects in ferrofluids*", J. Magn. Magn. Mater. **201** (1999) 170–173.

[5] Pu S., Bai X., and Wang L., "*Temperature dependence of photonic crystals based on thermoresponsive magnetic fluids*", J. Magn. Magn. Mater. **323** (2011) 2866–2871.

[6] Pu S., Chen X., Chen Y., Xu Y., Liao W., Chen L., and Xia Y., "*Fiber-optic evanescent field modulator using a magnetic fluid as the cladding*", J. Appl. Phys. **99** (2006) 093516.

[7] Miao Y., Wu J., Lin W., Zhang K., Yuan Y., Song B., Zhang H., Liu B., and Yao J., "*Magnetic field tunability of optical microfiber taper integrated with ferrofluid*", Opt. Express **21** (2013) 29914.

[8] Rodriguez-Schwendtner E., Navarrete M.-C., Diaz-Herrera N., Gonzalez-Cano A., and Esteban O., "*Advanced Plasmonic Fiber-Optic Sensor for High Sensitivity Measurement of Magnetic Field*", IEEE Sens. J. **19** (2019) 7355–7364.

[9] Luo L., Pu S., Dong S., and Tang J., "*Fiber-optic magnetic field sensor using magnetic fluid as the cladding*", Sensors Actuators A Phys. **236** (2015) 67–72.

[10] Haider T., "*A Review of Magneto-Optic Effects and Its Application*", Int. J. Electromagn. Appl. **7** (2017) 17–24.

[11] Sanz-Felipe A. and Martín J.C., "Ferrofluids with high dynamic ranges of optical transmission," in *Proceedings of SPIE - The International Society for Optical Engineering* (2017), Vol. 10453, p. 10453P.

[12] Chen L., Li J., Qiu X., Lin Y., Liu X., Miao H., and Fu J., "*Magneto-optical effect in a system of colloidal particle having anisotropic dielectric property*", Opt. Commun. **316** (2014) 146–151.

[13] Laskar J.M., Philip J., and Raj B., "*Experimental investigation of magnetic-field-induced aggregation kinetics in nonaqueous ferrofluids*", Phys. Rev. E **82** (2010) 021402.

[14] Horng H.E., Hong C.-Y., Yang S.Y., and Yang H.C., "*Novel properties and applications in magnetic fluids*", J. Phys. Chem. Solids **62** (2001) 1749–1764.

[15] Wu K.T., Yao Y.D., and Huang H.K., "*Comparison of dynamic and optical properties of Fe3O4 ferrofluid emulsion in water and oleic acid under magnetic field*", J. Magn. Magn. Mater. **209** (2000) 246–248.

[16] Laskar J.M., Philip J., and Raj B., "*Experimental evidence for reversible zippering of chains in magnetic nanofluids under external magnetic fields*", Phys. Rev. E **80** (2009) 041401.

[17] Sakhnini L. and El-Hilo M., "*Time dependence of light transmission in nanoparticle*

ferrofluids", J. Magn. Magn. Mater. **322** (2010) 1669–1672.
[18] Eloi M.T.A., Santos J.L., Morais P.C., and Bakuzis A.F., "*Field-induced columnar transition of biocompatible magnetic colloids: An aging study by magnetotransmissivity*", Phys. Rev. E **82** (2010) 021407.
[19] Rao G.N., Yao Y.D., Chen Y.L., Wu K.T., and Chen J.W., "*Particle size and magnetic field-induced optical properties of magnetic fluid nanoparticles*", Phys. Rev. E **72** (2005) 031408.
[20] Wu K.T., Yao Y.D., Wang C.R.C., Chen P.F., and Yeh E.T., "*Magnetic field induced optical transmission study in an iron nanoparticle ferrofluid*", J. Appl. Phys. **85** (1999) 5959–5961.
[21] Yang S.Y., Chiu Y.P., Jeang B.Y., Horng H.E., Hong C.-Y., and Yang H.C., "*Origin of field-dependent optical transmission of magnetic fluid films*", Appl. Phys. Lett. **79** (2001) 2372–2374.
[22] Lv R., Zhao Y., Xu N., and Li H., "*Research on the microstructure and transmission characteristics of magnetic fluids film based on the Monte Carlo method*", J. Magn. Magn. Mater. **337**–**338** (2013) 23–28.
[23] Sanz-Felipe Á. and Martín J.C., "*Numerical method for analysis of the correlation between ferrofluid optical transmission and its intrinsic properties*", J. Magn. Magn. Mater. **474** (2019).
[24] Sanz-Felipe Á. and Martín J.C., "*Analysis of the optical transmission of a ferrofluid by an electromagnetic mixture law*", J. Phys. D. Appl. Phys. **51** (2018) 135001.
[25] Bakuzis A.F., Branquinho L.C., Castro L.L., Eloi M.T.A., and Miotto R., "*Chain formation and aging process in biocompatible polydisperse ferrofluids: Experimental investigation and Monte Carlo simulations*", Adv. Colloid Interface Sci. **191**–**192** (2013) 1–21.
[26] Van de Hulst H.C., "*Light Scattering by Small Particles*" (New York: Dover Publications, Inc., 1981).
[27] Querry M.R., "*Optical Constants*" (Contractor Report CRDC-CR-85034 Univertisty of Missouri, 1985).
[28] Kedenburg S., Vieweg M., Gissibl T., and Giessen H., "*Linear refractive index and absorption measurements of nonlinear optical liquids in the visible and near-infrared spectral region*", Opt. Mater. Express **2** (2012) 1588.
[29] Shiratsu T. and Yao H., "*Size dependence of magneto-optical activity in silver nanoparticles with dimensions between 10 and 60 nm studied by MCD spectroscopy*", Phys. Chem. Chem. Phys. **20** (2018) 4269–4276.
[30] Menéndez J.L., Bescós B., Armelles G., Serna R., Gonzalo J., Doole R., Petford-Long A.K., and Alonso M.I., "*Optical and magneto-optical properties of Fe nanoparticles*", Phys. Rev. B **65** (2002) 205413.